
RetroGFN: Diverse and Feasible Retrosynthesis using GFlowNets

**Piotr Gaiński^{1,2}, Michał Koziarski^{3,4}, Krzysztof Maziarz⁵,
Marwin Segler⁵, Jacek Tabor¹, Marek Śmieja¹,**

¹ Jagiellonian University, Faculty of Mathematics and Computer Science, Krakow, Poland,

² Jagiellonian University, Doctoral School of Exact and Natural Sciences, Krakow, Poland,

³ Mila – Québec AI Institute, Montréal, Canada

⁴ Université de Montréal, Montréal, Canada

⁵ Microsoft Research, Cambridge, United Kingdom

piotr.gainski@doctoral.uj.edu.pl

Abstract

Single-step retrosynthesis aims to predict a set of reactions that lead to the creation of a target molecule, which is a crucial task in molecular discovery. Although a target molecule can often be synthesized with multiple different reactions, it is not clear how to verify the feasibility of a reaction, because the available datasets cover only a tiny fraction of the possible solutions. Consequently, the existing models are not encouraged to explore the space of possible reactions sufficiently. In this paper, we propose a novel single-step retrosynthesis model, RetroGFN, that can explore outside the limited dataset and return a diverse set of feasible reactions by leveraging a feasibility proxy model during the training. We show that RetroGFN achieves competitive results on standard top-k accuracy while outperforming existing methods on round-trip accuracy. Moreover, we provide empirical arguments in favor of using round-trip accuracy which expands the notion of feasibility with respect to the standard top-k accuracy metric.

1 Introduction

The rising interest in machine learning led to the development of many deep generative models for *de novo* drug design [1–5]. Such approaches can propose novel molecules with promising properties (e.g. high binding affinity score) predicted by other machine learning models [6–10], however, these virtual compounds eventually need to be synthesized and evaluated in the wet lab. This motivates the development of reliable (retro)synthesis planning algorithms able to design a synthesis route for an input molecule. Retrosynthesis aims to recursively decompose a target compound into simpler molecules forming a synthesis tree. The leaves of the tree are purchasable molecules from which the synthesis process can start and the tree itself is a synthesis recipe. By going bottom-up the tree and performing reactions defined by the tree nodes, one will eventually obtain the target molecule. The construction of such a tree usually consists of two components: a single-step retrosynthesis model that decomposes a molecule [11–16], and a multi-step planning algorithm that guides the recursive decomposition to obtain the full synthesis tree [17, 18, 16, 19–23]. In this paper, we focus on single-step retrosynthesis, which predicts a reaction that is likely to synthesize a given molecule.

In practice, many feasible reactions can lead to a given product. Since the success of a synthesis plan depends on factors that may vary over time (e.g. the availability or cost of reactants), the retrosynthesis model should ideally return all possible reactions. In other words, we would like to produce a diverse set of feasible reactions leading to the requested product. However, the available datasets cover only a fraction of feasible reactions, so for many of the included products, a lot of

alternative reactions are missing. This limitation of current reaction datasets causes two major issues that we address in this paper.

First, the typical evaluation of retrosynthesis models involves the use of top-k accuracy, which verifies how many top-k reactions returned by the model are included in a given dataset. Our analysis performed on the USPTO-50k test split [24, 12, 25] reveals that on average more than 100 feasible reactions returned by the examined retrosynthesis models are ignored by top-k accuracy (see Figure 1). Since it is practically impossible to include all possible reactions in a finite dataset, one remedy relies on employing a machine learning model, which reliably assesses the reaction feasibility. This approach is applied in round-trip accuracy, a less exploited alternative to the top-k accuracy metric. Our experimental study demonstrates that replacing top-k accuracy with top-k round-trip accuracy decreases the number of ignored reactions to less than 20 elements (Figure 1) while being robust to non-trivially unfeasible reactions (Figure 2). In consequence, round-trip accuracy should be taken into account as a complementary metric to standard top-k accuracy. We recommend reporting it in future papers to make model evaluation more comprehensive (see Section 3 for detailed analysis).

Second, since typical evaluation relies on using top-k accuracy (instead of round-trip accuracy), the existing retrosynthesis models are not encouraged to explore the space of feasible reactions well. Taking inspiration from the construction of round-trip accuracy, we employ a machine learning model, which rewards the retrosynthesis model for returning highly feasible reactions (not only those included in a fixed dataset). The main contribution of the paper is the development of a RetroGFN model that can explore beyond the dataset and return a diverse set of feasible reactions (Section 4). RetroGFN is based on the recent GFlowNet framework [26, 27] which enables exploration of the solution space and sampling from that space with probability proportional to the reward function, e.g., reaction feasibility. In consequence, GFlowNets can sample a large number of highly scored and diverse solutions. Our RetroGFN model leverages this property, sampling a large number of feasible reactions. It outperforms existing methods on the round-trip accuracy metric while achieving competitive results on the top-k accuracy.

To summarize, our contributions are:

- We provide empirical arguments for the importance of reporting the round-trip accuracy in the single-step retrosynthesis model evaluation (Section 3).
- We develop RetroGFN: a model based on the GFlowNet framework that generates diverse and feasible reactions. To our knowledge, we are the first to adapt GFlowNets for retrosynthesis (Section 4). We make the code publicly available¹.
- We benchmark the state-of-the-art single-step retrosynthesis models and show that our RetroGFN outperforms all considered models on the round-trip accuracy while achieving competitive results on the top-k accuracy (Section 5).

2 Related Work

Single-step Retrosynthesis. The single-step retrosynthesis problem is well-known in the drug-discovery community. The methods in this field can be roughly divided into template-based and template-free. The former are based on reaction templates (also called rules, see Figure 3), which describe the graph-level transformation of molecules that are encountered in the reactions [11, 12, 14, 28]. Templates provide a strong inductive bias as they form a fixed set of possible transformations that the retrosynthesis model can perform. Template-free approaches, on the other hand, do not rely on a template and aim to generate the transformation of the product (the change of the bonds and atoms between reactants and product) [29–33] or generate the product from scratch [34, 16, 35, 36]. Our RetroGFN is a template-based model, but it is not limited to a fixed set of templates as it composes them using pre-defined patterns. The template composition process was inspired by RetroComposer [37] but remains substantially different: we implement the generation process in the GFlowNets framework; we use more general patterns; we parametrize the second phase to be order-invariant; we guarantee the second phase ends with product and reactant patterns that can be mapped; and finally, we map the atoms using a machine learning model (while RetroComposer uses a heuristic).

GFlowNets. GFlowNets [27] are a type of generative methods devoted to sampling from high-dimensional distributions. GFlowNets were originally proposed as an alternative to MCMC (offering

¹<https://github.com/gmum/RetroGFN>

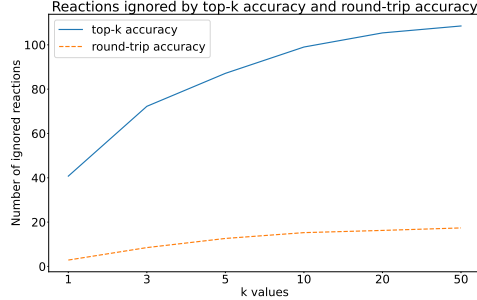


Figure 1: The average number of feasible reactions returned by a retrosynthesis model within its top- k predictions but ignored by top- k accuracy and top- k round-trip accuracy metrics on the USPTO-50k test split. The results are averaged over all models considered in this paper. Ground-truth reaction feasibility was assessed by checking for their presence in USPTO-MIT. We observe that round-trip accuracy treats almost all reactions ignored by top- k accuracy as feasible.

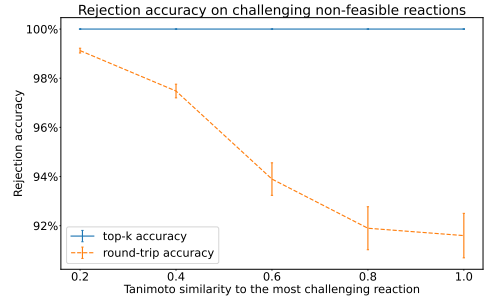


Figure 2: The accuracy of rejecting challenging non-feasible reactions. By definition, the top- k accuracy rejects all non-feasible reactions, while round-trip accuracy treats some portion of them as feasible as it assesses the feasibility with a machine learning model. We observe that even for the most tricky non-feasible reactions, the round-trip accuracy will likely not consider them feasible. Error bars are binomial proportion confidence intervals for $p = 0.05$.

the benefits of amortization) and reinforcement learning (displaying a mode-seeking behavior, that is the ability to discover multiple diverse modes), and later shown to be equivalent with special cases of other generative methods [38, 39]. The diversity, in particular, is a desired property in multiple scientific discovery tasks [40], including molecule [26, 41–43], biological sequence [26, 44], crystal [45], conformer [46] and DNA-encoded library [47] generation tasks. Importantly, from a scientific discovery standpoint, GFlowNets have also been used in the active learning context, both in the multi-objective [44] and multi-fidelity [48] settings.

3 Importance of Round-Trip Accuracy

In this section, we set up the single-step retrosynthesis problem, discuss the limitations of the widely used top- k accuracy metric, and argue for the relevance of the round-trip accuracy.

3.1 Single-Step Retrosynthesis

Single-step retrosynthesis is focused on predicting reactions that could lead to the given product (see Figure 3(a)). The retrosynthesis model is evaluated with a reaction dataset $D = \{(R_1, p_1), \dots, (R_n, p_n)\}$ containing reaction tuples where p_i denotes a product and R_i is a set of reactants that can synthesize the product p_i . During inference, the model is requested to return at most k reactions for every product from the dataset, which are expected to be sorted from the most to the least probable.

3.2 Limitations of Top- k Accuracy

Top- k accuracy is one of the most widely used metrics in retrosynthesis. To calculate it for the entire dataset, we first compute the support function F_{ACC} for every product p , which informs whether the ground-truth reaction was found in top k results returned by the model f :

$$F_{ACC}(f, p, k) = \mathbb{1}[\exists_{i \leq k} (f(p)_i, p) \in D], \quad (1)$$

where $f(p)_i$ is the i -th set of reactants proposed by the model for product p . Top- k accuracy denotes the portion of ground-truth reactions that were retrieved by the model and can be written as $ACC(f, k) = \frac{1}{n} \sum_{i=1}^n F_{ACC}(f, p_i, k)$.

Top-k accuracy works under the assumption that all sensible reactions for a given product are contained in the dataset. However, since there are often many different ways to make product, and it would be too expensive to try all of them. Therefore, real datasets are highly incomplete. In particular, it turns out that this assumption is not true for the USPTO-50k dataset [49, 24] which is the most widely used benchmark in the retrosynthesis community. To showcase that, we gathered all reactions returned by any of the considered retrosynthesis models (see Section 5) that are not included in USPTO-50k. Among 8409 reactions ranked top-1 by any considered model, 76 of them can be found in the USPTO-MIT dataset [25]. While top-k accuracy ignores these feasible reactions, the round-trip accuracy can account for a significant portion of them (see Figure 1).

3.3 Relevance of Round-Trip Accuracy

The top-k round-trip metric uses the wider notion of feasibility than top-k accuracy. For a single product, the top-k round-trip accuracy value denotes the percentage of feasible reactions among top k reactions returned by the machine learning model. The feasibility is estimated with a forward reaction prediction model F which is a fine-tuned Chemformer [34] (see Section 5.1). The exact formula for top-k round-trip accuracy calculated on a product p and retrosynthesis model f is given by:

$$F_{\text{Round}}(f, p, k) = \frac{1}{k} \sum_{i=1}^k \mathbb{1}[p \in F(f(p)_i)], \quad (2)$$

where $F(f(p)_i)$ is the set of products predicted by the forward model F for a set of reactants $f(p)_i$. In other words, the metric measures how many reactions proposed by a backward model f can be back-translated by a forward model F . We report the top-k round-trip accuracy for the entire dataset D , which can be written as $\text{Round}(f, k) = \frac{1}{n} \sum_i^n F_{\text{Round}}(f, p_i, k)$. Therefore, round-trip accuracy assesses both the diversity and feasibility of the returned reactions.

Figure 1 shows the ratio of feasible reactions ignored by top-k accuracy and round-trip accuracy. The metrics were computed on the USPTO-50k dataset and the "real" feasibility was assessed with USPTO-MIT. Note that the number of ignored feasible reactions is highly underestimated as USPTO-MIT is by no means exhaustive. The space of all reactions is enormous and even simple manipulations of leaving groups of reactants (e.g. changing Cl to Br) are likely to result in a lot of feasible reactions that were not screened in the wet lab before. While all the feasible reactions cannot be included in the dataset directly, the round-trip accuracy can account for some portion of them by leveraging the generalization properties of deep learning. The fact that our round-trip accuracy can account for strictly more feasible reactions than top-k accuracy is essential in the context of drug design, even at the cost of the increased number of non-feasible reactions accounted as feasible. It is because the profit lost caused by the inability to synthesize a drug is drastically higher than the cost of performing an unsuccessful synthesis experiment [50].

3.4 Reliability of Round-Trip Accuracy

To assess the reliability of the round-trip accuracy, we want to estimate what percentage of non-feasible reactions the round-trip accuracy will treat as feasible (we call this metric acceptance accuracy). The problem with constructing a set of non-feasible reactions is that they are very rarely reported in the literature. All reaction from USPTO-50k and USPTO-MIT datasets that we consider in that paper consists only of feasible reactions. Therefore, to obtain non-feasible reactions, we assume that for every set of reactants from the USPTO-MIT all of its possible outcomes were reported. Under this assumption, we can create a non-feasible reaction by taking a set of reactants from USPTO-MIT and a product that is not a possible outcome. We create an initial set of such reactions by applying random forward templates to the m reactants from USPTO-MIT (test split). Then we select a subset C of size $m/10$ of obtained reactions so that all reactions have distinct products and reactants. Then, for every reaction $(r, p) \in C$, we gather 9 sets of reactants from USPTO-MIT with possibly high Tanimoto similarity to r and add them to C . As a result, for every product p from C , we have a set of 10 corresponding reactions that are non-feasible in a non-trivial way. We additionally ensure that the sets of reactants are distinct across the reactions. If a set of reactants were shared between some reactions, then only one of those reactions would be accepted by a forward model, artificially increasing the acceptance accuracy.

The acceptance accuracy of round-trip accuracy (and underlying forward model) is reported in Figure 2. We see that the forward model accurately rejects even the most challenging reactions obtained by the forward reaction template application.

3.5 Generalization of Round-Trip Accuracy

Round-trip accuracy can be generalized to be able to use a wider class of machine learning models as a reaction feasibility proxy. We propose such a generalized metric in Appendix B and evaluate the baseline models on it.

4 RetroGFN

RetroGFN is a single-step retrosynthesis model, meaning it predicts a set of molecules that could react to a given target product (see Figure 3 a)). A product is represented as an annotated graph $G = (V, T, E)$, where nodes $V = \{v_1, v_2, \dots, v_n\}$ correspond to the molecule’s atoms along with associated atom symbols (types) T , and edges E are bonds. Additionally, each node and edge have an associated vector of features that will be used when embedding a molecule.

4.1 Reaction Templates and Patterns

Several existing single-step retrosynthesis models, including ours, work on the (backward) reaction templates. A reaction template can be seen as a regular expression on graphs (see Figure 3). It describes the transformation of a product into the reactants and consists of the product pattern (left side of the regular expression) and a set of reactants’ patterns (right side). The atoms of the product pattern are mapped to atoms of reactants’ patterns. Reaction templates provide a strong inductive bias to the model while limiting it to a fixed set of possible transformations. However, we extend the covered reaction space by introducing a template composition process inspired by RetroComposer [37]. In this approach, we choose the reaction center where the template is going to be applied and compose a concrete template step by step using the building blocks, called patterns.

We extract the templates from the train split of USPTO-50k, following [51]. Each template is then split into product and reactant patterns (see Figure 3 b)). We denote a set of all encountered product patterns PPS and an analogous set of reactant patterns RPS . The patterns do not include any molecular regular expression (SMARTS) and can be represented similarly to molecules - as annotated graphs.

4.2 Generation Process

Given a product, our RetroGFN composes an appropriate template in three phases:

1. The first phase determines a reaction center: a product pattern matched the product.
2. The second phase gathers the reactant patterns.
3. The third phase constructs atom mapping between the atoms of the product pattern and the reactants’ patterns.

In the end, the obtained template is applied to the given product and results in a final set of reactants. Figure 4 shows an example of the composition process while a detailed description of each phase can be found further in the section.

The core component of a GFlowNet model is a forward policy $P_F(a|s)$ describing the probability of taking action a in the state s . The generation process samples a sequence of states and actions $\tau = (s_1, a_1, \dots, s_k, a_k, t)$ called a trajectory, where t is a terminal state. In RetroGFN, an initial state

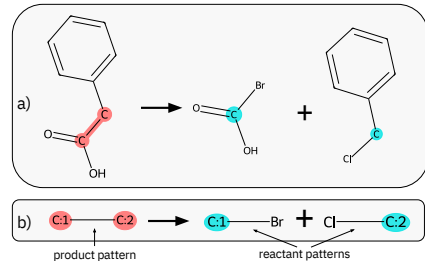


Figure 3: Illustration of a single-step retrosynthesis (a), and a corresponding reaction template (b). Atoms from a product pattern on the left side of the template are mapped to atoms from reactant patterns on the right side (red C: i is mapped to blue C: i).

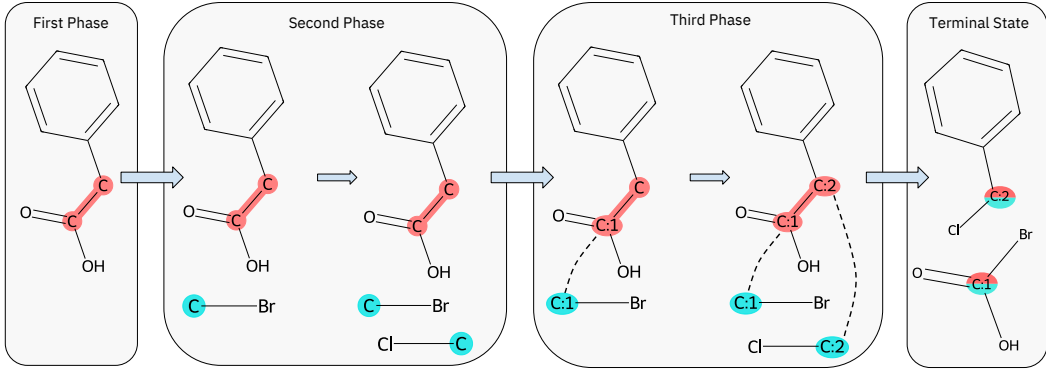


Figure 4: Illustration of the template composition process in RetroGFN for an input product. In the first phase, a product pattern and its concrete match to the atoms of the product is chosen. In the second phase, reactant patterns are gathered until all mappable atoms of the product pattern (highlighted red) can be mapped to mappable atoms of the reactant pattern (highlighted blue). In the third phase, the mapping between mappable product and reactant patterns is created and the obtained template is applied resulting in the reactants.

s_1 is an input product, the intermediate states s_i correspond to the partially constructed template, and the terminal state t stores a final template along with a result of its application to the product. We group the states into three phases and the specific definition of $P_F(a|s)$ depends on the phase i :

$$P_F^i(a|s) = \frac{\exp(\text{score}_i(s, a)\alpha)}{\sum_{a' \in A^i(s)} \exp(\text{score}_i(s, a')\alpha)},$$

where score_i is a phase-specific score function parameterized with a neural network and $A^i(s)$ is a set of possible actions that can be taken from s in the i -th phase. The policy is simply a softmax with temperature coefficient α over the scores of all possible actions $A^i(s)$.

Score functions for all the phases share a common Graph Neural Network (GNN) encoder, denoted as gnn_1 that given a product $p = (V, E, T)$, embeds its nodes' features: $\text{gnn}_1(p) \in \mathbb{R}^{n \times d}$, where n is the number of product nodes and d is the embedding size. We overload the notation and let $\text{gnn}_1(v_j)$ denote the embedding of a product node $v_j \in V$. The GNN architecture we use is similar to the one from LocalRetro: a stack of MPNN layers with a single Transformer layer [52] on top. Details can be found in the Appendix A.

First Phase. A state s in the first phase is an input product p . The action space $A^1(s)$ contains all possible atom matchings of product patterns from PPS to the product p . An action $a \in A^1(s)$ contains the matched product pattern $pp \in PPS$ and the matched atom indices $I = \{i_1, \dots, i_m\}$. The value of i_j is an index of the product atom matched with j -th product pattern atom. To compute the $\text{score}_1(s, a)$, we aggregate the representation of matched product's nodes and put them into multi-layer perceptron $\text{MLP}_1 : \mathbb{R}^d \rightarrow \mathbb{R}$:

$$\text{score}_1(s, a) = \text{MLP}_1 \left(\sum_{i \in I} \text{gnn}_1(v_i) \right).$$

After the action is chosen and applied, the generation process transitions directly to the second phase.

Second Phase. The second phase iteratively adds reactant patterns to the composed template. At the beginning of the phase, the list of reactant patterns is empty. The second phase action a is a reactant pattern $rp_j \in RPS$ that is going to be added to the template. The $\text{score}_2(s, a)$ concatenates the information from the previous phase and the reactant patterns collected so far (denoted as R) and feeds it to $\text{MLP}_2 : \mathbb{R}^{3d} \rightarrow \mathbb{R}^{|RPS|}$ that predicts the score for all the reactant patterns in RPS :

$$\text{score}_2(s, a) = \text{MLP}_2 \left(\sum_{i \in I} \text{gnn}_1(v_i) \mid \text{E}_{PPS}(pp) \mid \sum_{rp \in R} \text{E}_{RPS}(rp) \right)_j.$$

Here we select the j th score returned by the MLP_2 as it corresponds to rp_j reactant pattern from the action. Index embedding $e = \text{E}_A(a)$ is a function that looks up the index of the element a in the set A and assigns the index a learnable embedding $e \in \mathbb{R}^d$ (e.g. E_{PPS} assign a

unique learnable embedding to every $pp \in PPS$). At the end of this phase, we want to be sure that every atom from the product pattern can be mapped to some atom of the reactant pattern. Originally, each pattern had some atom mapping in the template it comes from (see Figure 3). Although those explicit mappings are inadequate in the novel-composed template, we can leverage the knowledge that an atom was originally mapped. For every pattern, we construct a set of mappable atoms that consists of the pattern’s atoms that were mapped in the original template (see Figure 5). The composed template is allowed to map only the mappable atoms. We ensure that all mappable atoms in the composed template can be mapped by properly restricting the action space $A^2(s)$.

Third Phase. The third phase creates a mapping between atoms of product and reactant patterns. An action a is an atom mapping $(j, k, l) \in M$ that links the j -th node from the product pattern pp with the l -th mappable node of the k -th reactant pattern from the list of reactant patterns R . The $\text{score}_3(s, a)$ is given with the formula:

$$\text{score}_3(s, a) = \text{MLP}_3(\text{gnn}_1(v_{ij}) \mid \text{gnn}_2(v_{kl})),$$

where v_{ij} is a product node matched with the j -th node of the product pattern, and v_{kl} is the l -th node of the k -th reactant pattern from R . To embed the reactant pattern nodes, we introduce a GNN gnn_2 with the same architecture as gnn_1 . The action space $A^3(s)$ contains all possible atom mappings. We call an atom mapping between two nodes possible when the atom symbols of the nodes are the same and neither of the nodes was previously mapped. The third phase ends when every node from the product pattern is mapped, resulting in a template that can be applied to the reaction center chosen in the first phase. The obtained reaction forms the terminal state t .

4.3 Training

We trained our RetroGFN with a modified version of Trajectory Balance Objective from [53], which for a trajectory $\tau = (s_1, a_1, s_2, a_2, \dots, s_k, a_k, t)$ is given with the formula:

$$\mathcal{L}(\tau) = \left(\log \frac{F(s_1) \prod_{i=1}^k P_F(a_i|s_i)}{R(t) P_B(a_k|t) \prod_{i=2}^k P_B(a_{i-1}|s_i)} \right)^2.$$

The main difference from the original formulation comes from the fact that our RetroGFN is conditioned [27, 54, 55, 44, 42] on the product from the initial state s_1 . Therefore, for every initial state, we estimate the incoming flow separately using $F(s_1)$ function which is essentially an index embedding $F(s) = E_P(s) \in \mathbb{R}$ that looks up the set of training products P and returns a learnable scalar (note that we only evaluate $F(s)$ during training). As a backward policy $P_B(a|s)$, we use a uniform distribution over the possible actions that could lead to state s . The reward is an exponential reward of the form $R(x) = \exp(\beta f(x))$ where f is a feasibility proxy. It can be a machine learning model that predicts the feasibility of a reaction or an indicator of whether the forward reaction prediction model was able to backtranslate the reaction x . In the main part of the paper, we evaluate the former, while experiments with the latter can be found in the Appendix B. The forward model used during training is distinct from the one used in the round-trip evaluation.

4.4 Inference

During inference, the retrosynthesis model is given a product and requested to output at most N reactions sorted from the most to least promising. RetroGFN samples the reactions using the trained forward policy $P_F(a|s)$ and orders them with the estimated probability. The probability of a reaction represented by a terminal state t is estimated by summing the probabilities of all sampled trajectories that end with t :

$$p(t) = \sum_{\tau: t \in \tau} \prod_{(s, a) \in \tau} P_F(a|s). \quad (3)$$

To increase the accuracy of the estimation, we sample $K \cdot N$ trajectories. We leave the exploration of other estimation methods for future work. The details on the architecture and hyperparameters of both training and inference can be found in the Appendix A.



Figure 5: Illustration of a pattern before (left) and after (right) mapping removal. The mappable atoms of the pattern are colored blue.

Table 1: Top-k round-trip accuracy results on USPTO-50k along with the standard deviation. The best results in every column are **bolded**. We observe that for $k > 1$ our RetroGFN consistently outperforms other methods.

method	top-1	top-3	top-5	top-10	top-20	top-50
GLN	92.2 ± 26.9	86.9 ± 23.8	83.7 ± 22.9	77.5 ± 22.6	67.3 ± 22.3	47.5 ± 20.6
MEGAN	87.0 ± 33.6	80.7 ± 28.1	76.5 ± 26.2	68.5 ± 24.8	58.2 ± 23.1	41.7 ± 21.0
MHNreact	90.8 ± 28.9	85.0 ± 24.8	80.5 ± 23.8	71.8 ± 23.1	59.9 ± 22.4	38.5 ± 19.2
LocalRetro	93.0 ± 25.6	87.6 ± 22.7	84.6 ± 21.6	79.3 ± 21.0	71.0 ± 21.2	54.2 ± 21.0
RootAligned	93.2 ± 25.2	84.6 ± 23.5	78.5 ± 23.1	67.5 ± 22.4	53.1 ± 19.4	27.0 ± 10.2
Chemformer	91.4 ± 28.0	58.2 ± 28.1	41.6 ± 24.6	24.0 ± 17.5	12.8 ± 10.8	5.3 ± 5.0
RetroKNN	92.8 ± 25.9	87.1 ± 22.8	83.8 ± 21.8	78.4 ± 20.9	69.8 ± 21.0	53.0 ± 20.1
RetroGFN	91.7 ± 27.6	88.2 ± 22.8	85.6 ± 21.5	81.1 ± 20.7	74.8 ± 20.3	63.5 ± 20.0

Table 2: Top-k accuracy results on USPTO-50k. The numbers in columns denote k values. The best results in every column are **bolded**. We observe that for $k > 3$ our RetroGFN achieves competitive results.

method	mrr	top-1	top-3	top-5	top-10	top-20	top-50
GLN	0.6509	52.4	74.6	81.2	88.0	91.8	93.1
MEGAN	0.6226	48.7	72.3	79.5	86.7	91.0	93.5
MHNreact	0.6356	50.6	73.1	80.1	86.4	90.3	92.6
LocalRetro	0.6565	51.5	76.5	84.3	91.0	94.9	96.7
RootAligned	0.6886	56.0	79.1	86.1	91.0	93.3	94.2
Chemformer	0.6312	55.0	70.9	73.7	75.4	75.9	76.0
RetroKNN	0.6834	55.3	77.9	85.0	91.5	91.6	96.6
RetroGFN	0.6308	49.2	73.3	81.1	88.0	92.2	95.3

5 Experiments

This section describes the benchmark methodology and results of our RetroGFN models compared to the current state-of-the-art. Tables 1, 2, 3 and 4 show that our RetroGFN outperforms all considered models on round-trip accuracy while achieving competitive results on the top-k accuracy.

5.1 Setup

Datasets. We compared the considered methods on two datasets: USPTO-50k, a default choice for benchmarking retrosynthesis models, and USPTO-MIT, which we use as a generalization benchmark for models trained on USPTO-50k. We used commonly used splits for both datasets [12, 25]. We refined the USPTO-MIT to ensure there is no overlap between it and the USPTO-50k train split.

Retrosynthesis Models. We compared our RetroGFN to well-known and recent state-of-the-art models: GLN [14], MEGAN [29], MHNreact [56], LocalRetro [51], RootAligned [30], RetroKNN [57], and Chemformer [34]. We used the wrappers of the original implementations and checkpoints from the Syntheseus repository¹. We used the evaluation procedure from Syntheseus that queries the model for 100 reactions, removes the duplicates, and truncates the list of reactions for every product to be no larger than 50. The same output was used both to calculate standard and round-trip metrics.

Forward Model. A forward (reaction prediction) model takes a set of reactants as an input and outputs a set of possible products. As a backbone, we used a pre-trained Chemformer model from [34]. We fine-tuned two forward models: Chemformer-Eval which was used to estimate the reaction feasibility in the round-trip accuracy (see Section 3) and Chemformer-Train which guided RetroGFN during the training (see Section 4). Chemformer-Train was fine-tuned on the train split of USPTO-50k, while Chemformer-Eval used both the train and test split of USPTO-50k.

¹<https://github.com/microsoft/syntheseus>

Table 3: Top-k round-trip accuracy on USPTO-MIT along with the standard deviation. The best results in every column are **bolded**. We observe that for $k > 3$ our RetroGFN consistently outperforms other methods.

method	top-1	top-3	top-5	top-10	top-20	top-50
GLN	83.5 ± 37.1	79.3 ± 31.0	76.3 ± 29.2	70.1 ± 27.3	60.3 ± 25.6	41.9 ± 21.9
MEGAN	81.9 ± 38.5	76.3 ± 31.4	72.3 ± 29.3	64.5 ± 27.0	54.2 ± 24.7	38.3 ± 21.4
MHNreact	82.8 ± 37.8	78.1 ± 30.8	74.4 ± 28.7	66.7 ± 26.7	55.2 ± 24.9	34.9 ± 20.1
LocalRetro	83.9 ± 36.7	80.3 ± 29.7	77.6 ± 27.7	72.5 ± 25.9	64.8 ± 24.6	49.1 ± 22.6
RootAligned	84.3 ± 36.4	77.6 ± 29.8	72.0 ± 27.8	62.0 ± 25.5	48.7 ± 21.2	24.8 ± 10.8
Chemformer	81.7 ± 38.7	53.5 ± 30.4	39.1 ± 25.4	23.0 ± 17.5	12.4 ± 10.5	5.1 ± 4.6
RetroKNN	83.3 ± 37.3	78.1 ± 30.2	74.1 ± 28.2	63.9 ± 27.0	44.0 ± 23.8	19.1 ± 12.0
RetroGFN	83.0 ± 37.5	80.3 ± 30.1	78.2 ± 28.0	73.9 ± 26.1	67.9 ± 24.6	56.9 ± 22.7

5.2 Results on USPTO-50k

The top-k round-trip accuracy results for USPTO-50k dataset can be found in Table 1. We observe that for $k > 1$ RetroGFN consistently outperforms all the models. The absolute and relative advantage of RetroGFN over the second-best model on top-k round-trip increases with k , indicating that the model can return a large set of diverse and feasible reactions. Note that the forward model used during the training of RetroGFN was trained on a different data split than the one used for evaluation. In Table 2, we can find standard top-k accuracy results. Our method performs competitively with state-of-the-art single-step retrosynthesis models, especially for larger values of k which is arguably more important for retrosynthesis search than $k = 1$.

We observe that for $k > 1$, our model consistently outperforms other models, producing plenty of feasible reactions. The absolute and relative advantage of RetroGFN over the second-best model on top-k FTC increases with k : from 3.6%p and 5.9% for $k=3$ to 9%p and 30.8% for $k=50$. The good results of RetroGFN on standard metrics and its exceptional performance on FTC evidence that one can greatly improve the results on FTC without sacrificing the performance on standard metrics. Interestingly, the Pearson correlation between top-k accuracy and top-k FTC for $k=1$ seems relatively high (corr=0.6, p -value=0.12), but it becomes insignificant for $k > 1$, indicating that the standard accuracy metric and FTC are complimentary (one can greatly improve upon the FTC without improving on standard metrics).

5.3 Generalization Results on USPTO-MIT

We evaluated the models trained on USPTO-50k further on the USPTO-MIT dataset to assess their generalization properties (Table 3 and 4). The evaluation of both standard and round-trip accuracy metrics echoes the results of USPTO-50k: RootAligned is the best on top-k accuracy, while our model achieves SOTA results on round-trip metrics. As in the USPTO-50k case, the absolute and relative advantage of RetroGFN over the second-best model on top-k round-trip increases with k .

5.4 Leveraging the Forward Model

In Appendix C, we study a simple model-agnostic way of leveraging the Chemformer-Train to maximize the results of the round-trip accuracy metric. While this approach significantly improves the round-trip accuracy results, it drastically decreases the standard top-k accuracy, especially for larger values of k . We leave the development of other methods of incorporating the Chemformer-Train model into the training pipeline for future work.

6 Conclusions

In this paper, we provided empirical arguments for the importance of reporting the round-trip accuracy in the single-step retrosynthesis model evaluation. Leveraging the GFlowNet framework which is designed for tasks where plenty of sensible solutions are desired, we developed a RetroGFN model that achieves competitive results on top-k accuracy and performs outstandingly on the top-k round-trip accuracy. We discuss the limitations of the paper in the Appendix D.

Table 4: Top-k accuracy results on USPTO-MIT. The best results in every column are **bolded**. We observe that our RetroGFN achieves competitive results.

method	mrr	top-1	top-3	top-5	top-10	top-20	top-50
GLN	0.4625	37.2	52.9	57.7	62.7	65.2	66.3
MEGAN	0.4647	37.0	53.4	58.8	63.7	66.8	68.9
MHNreact	0.4610	37.2	52.7	57.6	62.1	64.7	66.2
LocalRetro	0.4720	36.7	55.1	60.8	66.0	68.7	70.5
RootAligned	0.4960	40.2	56.8	61.7	66.1	68.5	69.5
Chemformer	0.4521	39.5	50.5	52.6	53.8	54.1	54.2
RetroKNN	0.4572	35.6	53.3	59.1	64.3	66.2	66.4
RetroGFN	0.4590	35.4	53.5	59.3	64.7	67.8	70.0

Acknowledgements

The research of P. Gaiński and M. Śmieja was supported by the National Science Centre (Poland), grant no. 2022/45/B/ST6/01117. The research of J. Tabor was supported by the Foundation for Polish Science co-financed by the European Union under the European Regional Development Fund in the POIR.04.04.00-00-14DE/18-00 project carried out within the Team-Net program. The research of M. Koziarski was supported by funding from CQDM Fonds d’Accélération des Collaborations en Santé (FACS) / Acuité Québec and Genentech. We gratefully acknowledge Poland’s high-performance Infrastructure PLGrid (ACK Cyfronet Athena, HPC) for providing computer facilities and support within computational grant no PLG/2023/016550. For the purpose of Open Access, the author has applied a CC-BY public copyright license to any Author Accepted Manuscript (AAM) version arising from this submission.

References

- [1] Marwin HS Segler, Thierry Kogej, Christian Tyrchan, and Mark P Waller. Generating focussed molecule libraries for drug discovery with recurrent neural networks. *arXiv preprint arXiv:1701.01329*, 2017.
- [2] Rafael Gómez-Bombarelli, Jennifer N Wei, David Duvenaud, José Miguel Hernández-Lobato, Benjamín Sánchez-Lengeling, Dennis Sheberla, Jorge Aguilera-Iparraguirre, Timothy D Hirzel, Ryan P Adams, and Alán Aspuru-Guzik. Automatic chemical design using a data-driven continuous representation of molecules. *ACS central science*, 4(2):268–276, 2018.
- [3] Łukasz Maziarka, Agnieszka Pocha, Jan Kaczmarczyk, Krzysztof Rataj, Tomasz Danel, and Michał Warchał. Mol-cyclegan: a generative model for molecular optimization. *Journal of Cheminformatics*, 12(1):1–18, 2020.
- [4] Krzysztof Maziarz, Henry Richard Jackson-Flux, Pashmina Cameron, Finton Sirockin, Nadine Schneider, Nikolaus Stiefl, Marwin Segler, and Marc Brockschmidt. Learning to extend molecular scaffolds with structural motifs. In *International Conference on Learning Representations*, 2022.
- [5] Joshua Meyers, Benedek Fabian, and Nathan Brown. De novo molecular design and generative models. *Drug Discovery Today*, 26(11):2707–2715, 2021.
- [6] W Patrick Walters and Regina Barzilay. Applications of deep learning in molecule generation and molecular property prediction. *Accounts of chemical research*, 54(2):263–270, 2020.
- [7] Piotr Gaiński, Michał Koziarski, Jacek Tabor, and Marek Śmieja. Chienn: Embracing molecular chirality with graph neural networks. In *Joint European Conference on Machine Learning and Knowledge Discovery in Databases*, pages 36–52. Springer, 2023.
- [8] Łukasz Maziarka, Dawid Majchrowski, Tomasz Danel, Piotr Gaiński, Jacek Tabor, Igor Podolak, Paweł Morkisz, and Stanisław Jastrzębski. Relative molecule self-attention transformer. *Journal of Cheminformatics*, 16(1):3, 2024.

- [9] Seyone Chithrananda, Gabriel Grand, and Bharath Ramsundar. Chemberta: large-scale self-supervised pretraining for molecular property prediction. *arXiv preprint arXiv:2010.09885*, 2020.
- [10] Shuangli Li, Jingbo Zhou, Tong Xu, Dejing Dou, and Hui Xiong. Geomgcl: Geometric graph contrastive learning for molecular property prediction. In *Proceedings of the AAAI conference on artificial intelligence*, volume 36, pages 4541–4549, 2022.
- [11] Marwin HS Segler and Mark P Waller. Neural-symbolic machine learning for retrosynthesis and reaction prediction. *Chemistry—A European Journal*, 23(25):5966–5971, 2017.
- [12] Connor W. Coley, Luke Rogers, William H. Green, and Klavs F. Jensen. Computer-assisted retrosynthesis based on molecular similarity. *ACS Central Science*, 3(12):1237–1245, 2017.
- [13] Bowen Liu, Bharath Ramsundar, Prasad Kawthekar, Jade Shi, Joseph Gomes, Quang Luu Nguyen, Stephen Ho, Jack Sloane, Paul Wender, and Vijay Pande. Retrosynthetic reaction prediction using neural sequence-to-sequence models. *ACS Central Science*, 3(10):1103–1113, 2017.
- [14] Hanjun Dai, Chengtao Li, Connor Coley, Bo Dai, and Le Song. Retrosynthesis prediction with conditional graph logic network. *Advances in Neural Information Processing Systems*, 32, 2019.
- [15] Ruoxi Sun, Hanjun Dai, Li Li, Steven Kearnes, and Bo Dai. Energy-based view of retrosynthesis. *arXiv preprint arXiv:2007.13437*, 2020.
- [16] Philippe Schwaller, Riccardo Petraglia, Valerio Zullo, Vishnu H Nair, Rico Andreas Haeuselmann, Riccardo Pisoni, Costas Bekas, Anna Iuliano, and Teodoro Laino. Predicting retrosynthetic pathways using transformer-based models and a hyper-graph exploration strategy. *Chemical science*, 11(12):3316–3325, 2020.
- [17] Marwin HS Segler, Mike Preuss, and Mark P Waller. Planning chemical syntheses with deep neural networks and symbolic ai. *Nature*, 555(7698):604–610, 2018.
- [18] Connor W Coley, Dale A Thomas III, Justin AM Lummiss, Jonathan N Jaworski, Christopher P Breen, Victor Schultz, Travis Hart, Joshua S Fishman, Luke Rogers, Hanyu Gao, et al. A robotic platform for flow synthesis of organic compounds informed by ai planning. *Science*, 365(6453):eaax1566, 2019.
- [19] Binghong Chen, Chengtao Li, Hanjun Dai, and Le Song. Retro*: learning retrosynthetic planning with neural guided A* search. In *International Conference on Machine Learning*, pages 1608–1616. PMLR, 2020.
- [20] Shufang Xie, Rui Yan, Peng Han, Yingce Xia, Lijun Wu, Chenjuan Guo, Bin Yang, and Tao Qin. Retrograph: Retrosynthetic planning with graph search. In *Proceedings of the 28th ACM SIGKDD Conference on Knowledge Discovery and Data Mining*, pages 2120–2129, 2022.
- [21] Guoqing Liu, Di Xue, Shufang Xie, Yingce Xia, Austin Tripp, Krzysztof Maziarz, Marwin Segler, Tao Qin, Zongzhang Zhang, and Tie-Yan Liu. Retrosynthetic planning with dual value networks. *arXiv preprint arXiv:2301.13755*, 2023.
- [22] Austin Tripp, Krzysztof Maziarz, Sarah Lewis, Guoqing Liu, and Marwin Segler. Re-evaluating chemical synthesis planning algorithms. In *NeurIPS 2022 AI for Science: Progress and Promises*, 2022. URL <https://openreview.net/forum?id=8VLeT8DFeD>.
- [23] Austin Tripp, Krzysztof Maziarz, Sarah Lewis, Marwin Segler, and José Miguel Hernández-Lobato. Retro-fallback: retrosynthetic planning in an uncertain world. *arXiv preprint arXiv:2310.09270*, 2023.
- [24] Nadine Schneider, Nikolaus Stiefl, and Gregory A Landrum. What’s what: The (nearly) definitive guide to reaction role assignment. *Journal of chemical information and modeling*, 56(12):2336–2346, 2016.
- [25] Wengong Jin, Connor Coley, Regina Barzilay, and Tommi Jaakkola. Predicting organic reaction outcomes with weisfeiler-lehman network. *Advances in neural information processing systems*, 30, 2017.

- [26] Emmanuel Bengio, Moksh Jain, Maksym Korablyov, Doina Precup, and Yoshua Bengio. Flow network based generative models for non-iterative diverse candidate generation. *Advances in Neural Information Processing Systems*, 34:27381–27394, 2021.
- [27] Yoshua Bengio, Salem Lahlou, Tristan Deleu, Edward J Hu, Mo Tiwari, and Emmanuel Bengio. Gflownet foundations. *Journal of Machine Learning Research*, 24(210):1–55, 2023.
- [28] Javier L Baylon, Nicholas A Cilfone, Jeffrey R Gulcher, and Thomas W Chittenden. Enhancing retrosynthetic reaction prediction with deep learning using multiscale reaction classification. *Journal of chemical information and modeling*, 59(2):673–688, 2019.
- [29] Mikołaj Sacha, Mikołaj Błaz, Piotr Byrski, Paweł Dabrowski-Tumanski, Mikołaj Chrominski, Rafał Łoska, Paweł Włodarczyk-Pruszynski, and Stanisław Jastrzebski. Molecule edit graph attention network: modeling chemical reactions as sequences of graph edits. *Journal of Chemical Information and Modeling*, 61(7):3273–3284, 2021.
- [30] Zipeng Zhong, Jie Song, Zunlei Feng, Tiantao Liu, Lingxiang Jia, Shaolun Yao, Min Wu, Tingjun Hou, and Mingli Song. Root-aligned smiles: a tight representation for chemical reaction prediction. *Chemical Science*, 13(31):9023–9034, 2022.
- [31] Chaochao Yan, Qianggang Ding, Peilin Zhao, Shuangjia Zheng, Jinyu Yang, Yang Yu, and Junzhou Huang. Retroxpert: Decompose retrosynthesis prediction like a chemist. *Advances in Neural Information Processing Systems*, 33:11248–11258, 2020.
- [32] Vignesh Ram Somnath, Charlotte Bunne, Connor Coley, Andreas Krause, and Regina Barzilay. Learning graph models for retrosynthesis prediction. *Advances in Neural Information Processing Systems*, 34:9405–9415, 2021.
- [33] Xiaorui Wang, Yuquan Li, Jiezhong Qiu, Guangyong Chen, Huanxiang Liu, Benben Liao, Chang-Yu Hsieh, and Xiaojun Yao. Retroprime: A diverse, plausible and transformer-based method for single-step retrosynthesis predictions. *Chemical Engineering Journal*, 420:129845, 2021.
- [34] Ross Irwin, Spyridon Dimitriadis, Jiazen He, and Esben Jannik Bjerrum. Chemformer: a pre-trained transformer for computational chemistry. *Machine Learning: Science and Technology*, 3(1):015022, 2022.
- [35] Shuangjia Zheng, Jiahua Rao, Zhongyue Zhang, Jun Xu, and Yuedong Yang. Predicting retrosynthetic reactions using self-corrected transformer neural networks. *Journal of chemical information and modeling*, 60(1):47–55, 2019.
- [36] Kelong Mao, Xi Xiao, Tingyang Xu, Yu Rong, Junzhou Huang, and Peilin Zhao. Molecular graph enhanced transformer for retrosynthesis prediction. *Neurocomputing*, 457:193–202, 2021.
- [37] Chaochao Yan, Peilin Zhao, Chan Lu, Yang Yu, and Junzhou Huang. Retrocomposer: Composing templates for template-based retrosynthesis prediction. *Biomolecules*, 12(9):1325, 2022.
- [38] Nikolay Malkin, Salem Lahlou, Tristan Deleu, Xu Ji, Edward Hu, Katie Everett, Dinghuai Zhang, and Yoshua Bengio. Gflownets and variational inference. *arXiv preprint arXiv:2210.00580*, 2022.
- [39] Dinghuai Zhang, Ricky TQ Chen, Nikolay Malkin, and Yoshua Bengio. Unifying generative models with gflownets. *arXiv preprint arXiv:2209.02606*, 2022.
- [40] Moksh Jain, Tristan Deleu, Jason Hartford, Cheng-Hao Liu, Alex Hernandez-Garcia, and Yoshua Bengio. Gflownets for ai-driven scientific discovery. *Digital Discovery*, 2(3):557–577, 2023.
- [41] Andrei Cristian Nica, Moksh Jain, Emmanuel Bengio, Cheng-Hao Liu, Maksym Korablyov, Michael M Bronstein, and Yoshua Bengio. Evaluating generalization in gflownets for molecule design. In *ICLR2022 Machine Learning for Drug Discovery*, 2022.
- [42] Julien Roy, Pierre-Luc Bacon, Christopher Pal, and Emmanuel Bengio. Goal-conditioned gflownets for controllable multi-objective molecular design. *arXiv preprint arXiv:2306.04620*, 2023.

- [43] Michał Koziarski, Andrei Rekesh, Dmytro Shevchuk, Almer van der Sloot, Piotr Gaiński, Yoshua Bengio, Cheng-Hao Liu, Mike Tyers, and Robert A Batey. Rgfn: Synthesizable molecular generation using gflownets. *arXiv preprint arXiv:2406.08506*, 2024.
- [44] Moksh Jain, Sharath Chandra Raparthy, Alex Hernández-García, Jarrid Rector-Brooks, Yoshua Bengio, Santiago Miret, and Emmanuel Bengio. Multi-objective gflownets. In *International Conference on Machine Learning*, pages 14631–14653. PMLR, 2023.
- [45] Mila AI4Science, Alex Hernandez-Garcia, Alexandre Duval, Alexandra Volokhova, Yoshua Bengio, Divya Sharma, Pierre Luc Carrier, Michał Koziarski, and Victor Schmidt. Crystal-gfn: sampling crystals with desirable properties and constraints. *arXiv preprint arXiv:2310.04925*, 2023.
- [46] Alexandra Volokhova, Michał Koziarski, Alex Hernández-García, Cheng-Hao Liu, Santiago Miret, Pablo Lemos, Luca Thiede, Zichao Yan, Alán Aspuru-Guzik, and Yoshua Bengio. Towards equilibrium molecular conformation generation with gflownets. *Digital Discovery*, 3(5):1038–1047, 2024.
- [47] Michał Koziarski, Mohammed Abukalam, Vedant Shah, Louis Vaillancourt, Doris Alexandra Schuetz, Moksh Jain, Almer M van der Sloot, Mathieu Bourgey, Anne Marinier, and Yoshua Bengio. Towards dna-encoded library generation with gflownets. In *ICLR 2024 Workshop on Generative and Experimental Perspectives for Biomolecular Design*, 2024.
- [48] Alex Hernandez-Garcia, Nikita Saxena, Moksh Jain, Cheng-Hao Liu, and Yoshua Bengio. Multi-fidelity active learning with gflownets. *arXiv preprint arXiv:2306.11715*, 2023.
- [49] Daniel Mark Lowe. *Extraction of chemical structures and reactions from the literature*. PhD thesis, University of Cambridge, 2012.
- [50] Tal Burt, KS Button, HHZ Thom, RJ Noveck, and Marcus R Munafò. The burden of the “false-negatives” in clinical development: Analyses of current and alternative scenarios and corrective measures. *Clinical and translational science*, 10(6):470–479, 2017.
- [51] Shuan Chen and Yousung Jung. Deep retrosynthetic reaction prediction using local reactivity and global attention. *JACS Au*, 1(10):1612–1620, 2021.
- [52] Ashish Vaswani, Noam Shazeer, Niki Parmar, Jakob Uszkoreit, Llion Jones, Aidan N Gomez, Łukasz Kaiser, and Illia Polosukhin. Attention is all you need. *Advances in neural information processing systems*, 30, 2017.
- [53] Nikolay Malkin, Moksh Jain, Emmanuel Bengio, Chen Sun, and Yoshua Bengio. Trajectory balance: Improved credit assignment in gflownets. *Advances in Neural Information Processing Systems*, 35:5955–5967, 2022.
- [54] Ling Pan, Moksh Jain, Kanika Madan, and Yoshua Bengio. Pre-training and fine-tuning generative flow networks. *arXiv preprint arXiv:2310.03419*, 2023.
- [55] Minsu Kim, Joohwan Ko, Dinghuai Zhang, Ling Pan, Taeyoung Yun, Woochang Kim, Jinkyoo Park, and Yoshua Bengio. Learning to scale logits for temperature-conditional gflownets. *arXiv preprint arXiv:2310.02823*, 2023.
- [56] Philipp Seidl, Philipp Renz, Natalia Dyubankova, Paulo Neves, Jonas Verhoeven, Marwin Segler, Jörg K Wegner, Sepp Hochreiter, and Günter Klambauer. Modern hopfield networks for few-and zero-shot reaction template prediction. *arXiv preprint arXiv:2104.03279*, 2021.
- [57] Shufang Xie, Rui Yan, Junliang Guo, Yingce Xia, Lijun Wu, and Tao Qin. Retrosynthesis prediction with local template retrieval. In *Proceedings of the AAAI Conference on Artificial Intelligence*, 2023.
- [58] Steven Kearnes, Kevin McCloskey, Marc Berndl, Vijay Pande, and Patrick Riley. Molecular graph convolutions: moving beyond fingerprints. *Journal of computer-aided molecular design*, 30:595–608, 2016.

- [59] Minjie Wang, Da Zheng, Zihao Ye, Quan Gan, Mufei Li, Xiang Song, Jinjing Zhou, Chao Ma, Lingfan Yu, Yu Gai, et al. Deep graph library: A graph-centric, highly-performant package for graph neural networks. *arXiv preprint arXiv:1909.01315*, 2019.
- [60] Vijay Prakash Dwivedi, Anh Tuan Luu, Thomas Laurent, Yoshua Bengio, and Xavier Bresson. Graph neural networks with learnable structural and positional representations. *arXiv preprint arXiv:2110.07875*, 2021.
- [61] Justin Gilmer, Samuel S Schoenholz, Patrick F Riley, Oriol Vinyals, and George E Dahl. Neural message passing for quantum chemistry. In *International conference on machine learning*, pages 1263–1272. PMLR, 2017.
- [62] Max W Shen, Emmanuel Bengio, Ehsan Hajiramezanali, Andreas Loukas, Kyunghyun Cho, and Tommaso Biancalani. Towards understanding and improving gflownet training. *arXiv preprint arXiv:2305.07170*, 2023.
- [63] William Fedus, Prajit Ramachandran, Rishabh Agarwal, Yoshua Bengio, Hugo Larochelle, Mark Rowland, and Will Dabney. Revisiting fundamentals of experience replay. In *International Conference on Machine Learning*, pages 3061–3071. PMLR, 2020.
- [64] Moksh Jain, Emmanuel Bengio, Alex Hernandez-Garcia, Jarrid Rector-Brooks, Bonaventure FP Dossou, Chanakya Ajit Ekbote, Jie Fu, Tianyu Zhang, Michael Kilgour, Dinghuai Zhang, et al. Biological sequence design with gflownets. In *International Conference on Machine Learning*, pages 9786–9801. PMLR, 2022.
- [65] Diederik P Kingma and Jimmy Ba. Adam: A method for stochastic optimization. *arXiv preprint arXiv:1412.6980*, 2014.
- [66] Keyulu Xu, Weihua Hu, Jure Leskovec, and Stefanie Jegelka. How powerful are graph neural networks? *arXiv preprint arXiv:1810.00826*, 2018.

A RetroGFN Details

All neural networks in RetroGFN used the same hidden dimension $h = 200$. To obtain initial node and edge features for products, we used featurization from [58] implemented in the DGL library [59]. For the reactant pattern, we used the same edge featurization and a custom node featurization that accounted for atom type, degree, aromaticity, whether the atom was mapped in the original template, relative charge difference between product and reactant atom in the original template, and analogous implicit hydrogen difference. The node features for both products and reactant patterns were enriched with random walk positional encoding [60] of size $n_{\text{random_walk}} = 16$.

Product node encoder gnn_1 consists of $\text{num_layer_1} = 4$ layers of the MPNN convolution [61] and one Transformer layer with $\text{num_heads} = 8$. The reactant pattern encoder differs only in the number of layers $\text{num_layer_2} = 3$. Multi-layer perceptrons $\text{MLP}_1, \text{MLP}_2, \text{MLP}_3$ had one hidden layer (with hidden dimension h) and used the GeLU activation function.

During training, we used a combination of three sampling methods: 1) standard exploratory sampling from the forward policy P_F with some ϵ probability of taking random actions, 2) backward sampling from replay buffer [62–64], and 3) backward sampling from the dataset D . Backward sampling starts with a terminal state and samples the trajectory in the backward direction using the backward policy.

During the training probability of taking random action in the forward policy was set to $\epsilon = 0.05$, the number of sampled forward trajectories in the batch was $n_{\text{forward}} = 16$, and the analogous numbers for backward dataset trajectories and backward replay buffer trajectories were $n_{\text{dataset}} = 96$ and $n_{\text{replay}} = 16$. The model was trained with Adam optimizer [65] with a learning rate $lr = 0.0005$ (with other parameters set to default values in the torch implementation) for $n_{\text{iterations}} = 25000$ iterations. In the evaluation, the forward policy temperature was set to $\alpha = 0.7$. During the inference, we sampled $K \cdot N$ trajectories to accurately estimate the reaction probability. For USPTO-50k, we set $K = 20$ while for, due to limited computational resources, we set $K = 10$ for USPTO-MIT.

All the hyperparameters were chosen manually based on the top-k accuracy and round-trip accuracy estimated on the USPTO-50k validation split.

B Generalization of Round-Trip Accuracy

We propose a generalization of round-trip accuracy that allows to use of a wider class of machine-learning models to assess the reaction feasibility. We call this metric Feasible Thresholded Count (FTC). For a single product, the top-k FTC value denotes the percentage of feasible reactions among top k reactions returned by the model. The feasibility is estimated with an auxiliary model RFM described in further in this section. The exact formula for top-k FTC calculated on a product p and retrosynthesis model f is given by:

$$F_{\text{FTC}}(f, p, k) = \frac{1}{k} \sum_{i=1}^k \mathbb{1}[\text{RFM}(f(p)_i) \geq t], \quad (4)$$

where $\text{RFM}(f(p)_i) \in [0, 1]$ is the output of the reaction feasibility model for the i -th reaction proposed by f , and t is a feasibility threshold given by the user. We assume that $\text{RFM}(x) = 1$ for reaction $x \in D$. We report the top-k FTC for the entire dataset D , which can be written as $FTC(f, k) = \frac{1}{n} \sum_i^n F_{\text{FTC}}(f, p_i, k)$.

B.1 Reaction Feasibility Model (RFM)

The Reaction Feasibility Model (RFM) is a model that takes reaction x as an input and outputs its feasibility - probability that the reaction is feasible: $\text{RFM}(x) \in [0, 1]$. In this paper, we develop an RFM baseline that can be used as a benchmark in future work.

Architecture. Our RFM implementation consists of two GINE [66] Graph Neural Networks (GNN) with a Transformer [52] layer and attention pooling at the top that creates product and reactant embeddings which are then concatenated and fed into the MLP layer.

Checkpoints for USPTO-50k. To train the model, we augmented the USPTO-50k dataset with negative (non-feasible) reactions using two methods: 1) application of existing forward templates to

obtain a novel product from existing reactants, 2) swapping a product in the reaction with another product that is similar to the original one in terms of Tanimoto similarity. Such an approach ensured that the generated negative reactions are not trivially unfeasible (they use an existing template and/or the product is not strikingly different from the reactants), but still are very unlikely to occur in reality (the original reactants were reported to return a different product). We obtained a reaction feasibility dataset with a negative-to-positive ratio of 5:1. We trained two distinct checkpoints of feasibility models: RFM-Train-50k and RFM-Eval-50k. The RFM-Train was trained only on the train split of the reaction feasibility dataset and was then used to calculate the reward in the RetroGFN during the training.

B.2 Experiments

We trained the RetroGFN using the RFM-Train model as a feasibility proxy and compared it on top-k accuracy and our FTC metric. We used the same hyperparameters as in Appendix A, but with $n_{\text{dataset}} = 80$, $n_{\text{replay}} = 16$, $n_{\text{forward}} = 32$ and $\beta = 12$. The results (Tables 5, 6, 7 and 8) mimic the ones from the main paper: our RetroGFN outperforms the model on FTC metric while obtaining competitive results on the standard top-k accuracy. The experiments show that our RetroGFN can leverage any machine-learning feasibility proxy. We believe that training a reliable and powerful feasibility proxy is a promising direction for future work.

Table 5: Top-k FTC results on USPTO-50k along with the standard deviation for threshold $t = 0.9$. The best results in every column are **bolded**. We observe that for $k > 1$ our RetroGFN consistently outperforms other methods.

method	top-1	top-3	top-5	top-10	top-20	top-50
GLN	74.0 ± 43.9	57.4 ± 31.8	49.0 ± 28.2	38.1 ± 23.3	28.4 ± 18.9	16.4 ± 12.0
MEGAN	70.4 ± 45.7	54.2 ± 31.1	46.7 ± 27.4	37.3 ± 23.2	28.6 ± 18.9	18.5 ± 13.4
MHNreact	72.0 ± 44.9	54.1 ± 30.6	45.5 ± 26.3	35.0 ± 21.6	25.6 ± 17.2	14.3 ± 10.6
LocalRetro	73.4 ± 44.2	57.2 ± 30.6	49.8 ± 27.4	40.0 ± 23.6	31.4 ± 19.9	20.1 ± 13.6
RetroKNN	72.0 ± 44.9	54.7 ± 30.4	47.0 ± 26.6	35.7 ± 21.9	22.5 ± 15.6	9.5 ± 6.9
RootAligned	75.9 ± 42.8	57.2 ± 29.7	49.7 ± 27.2	40.3 ± 23.9	31.4 ± 19.9	16.1 ± 10.9
Chemformer	74.9 ± 43.4	41.5 ± 25.3	28.5 ± 19.5	15.7 ± 12.2	8.2 ± 7.2	3.4 ± 3.3
RetroGFN	72.4 ± 44.7	61.0 ± 31.9	54.1 ± 29.3	46.0 ± 26.6	38.9 ± 24.2	29.1 ± 19.5

Table 6: Top-k accuracy results on USPTO-50k. The numbers in columns denote k values. The best results in every column are **bolded**. We observe that for $k > 3$ our RetroGFN achieves competitive results.

method	MRR	top-1	top-3	top-5	top-10	top-20	top-50
GLN	0.6509	52.4	74.6	81.2	88.0	91.8	93.1
MEGAN	0.6226	48.7	72.3	79.5	86.7	91.0	93.5
MHNreact	0.6356	50.6	73.1	80.1	86.4	90.3	92.6
LocalRetro	0.6565	51.5	76.5	84.3	91.0	94.9	96.7
RetroKNN	0.6834	55.3	77.9	85.0	91.5	91.6	96.6
RootAligned	0.6886	56.0	79.1	86.1	91.0	93.3	94.2
Chemformer	0.6312	55.0	70.9	73.7	75.4	75.9	76.0
RetroGFN	0.6144	46.9	72.2	80.0	87.8	91.9	94.7

C Ablations

In this section we study a simple model-agnostic way of leveraging the Chemformer-Train to maximize the results of round-trip accuracy metric. The idea is to filter the results that are not backtranslated by the Chemformer-Train model during the evaluation. Tables 9 and 10 show that such an approach significantly improves the round-trip accuracy results, but with the costs of a drastic decrease of a standard top-k accuracy, especially for larger values of k .

Table 7: Top-k FTC results on USPTO-MIT along with the standard deviation for threshold $t = 0.9$. The best results in every column are **bolded**. We observe that for $k > 1$ our RetroGFN consistently outperforms other methods.

method	top-1	top-3	top-5	top-10	top-20	top-50
GLN	74.8 ± 43.4	64.2 ± 33.4	58.3 ± 30.2	49.7 ± 26.0	40.6 ± 21.9	27.6 ± 17.0
MEGAN	72.9 ± 44.5	61.5 ± 32.8	55.6 ± 29.3	47.2 ± 25.1	38.8 ± 21.2	27.1 ± 16.5
MHNreact	73.3 ± 44.2	61.7 ± 33.2	55.2 ± 29.5	46.1 ± 24.9	36.6 ± 20.9	22.7 ± 15.5
LocalRetro	76.3 ± 42.5	65.4 ± 32.2	59.4 ± 29.2	51.3 ± 25.4	42.9 ± 21.9	30.2 ± 16.9
RootAligned	77.6 ± 41.7	66.0 ± 31.5	60.0 ± 28.7	51.7 ± 25.3	42.4 ± 21.6	22.8 ± 12.7
Chemformer	73.8 ± 44.0	47.1 ± 29.5	34.2 ± 23.7	20.2 ± 16.3	11.0 ± 10.3	4.6 ± 5.0
RetroKNN	75.0 ± 43.3	62.9 ± 32.1	56.1 ± 28.7	45.1 ± 24.5	29.8 ± 18.9	12.8 ± 9.1
RetroGFN	77.4 ± 41.8	69.1 ± 32.5	64.5 ± 29.8	58.1 ± 26.8	51.7 ± 24.4	40.7 ± 20.2

Table 8: Top-k accuracy results on USPTO-MIT. The numbers in columns denote k values. The best results in every column are **bolded**. We observe that for $k > 3$ our RetroGFN achieves competitive results.

method	MRR	top-1	top-3	top-5	top-10	top-20	top-50
GLN	0.4480	35.6	51.5	56.5	61.6	64.2	65.3
MEGAN	0.4498	35.3	52.0	57.6	62.6	65.8	68.1
MHNreact	0.4451	35.3	51.3	56.4	60.9	63.7	65.2
LocalRetro	0.4636	36.0	54.2	59.9	65.1	67.9	69.7
RetroKNN	0.4491	34.9	52.5	58.2	63.5	65.3	65.5
RootAligned	0.4838	38.9	55.6	60.6	65.2	67.7	68.8
Chemformer	0.4362	37.8	49.1	51.2	52.5	52.9	52.9
RetroGFN	0.4375	33.1	51.3	57.5	63.3	66.7	68.9

Table 9: Top-k accuracy results on USPTO-50k for models that use the Chemformer-Train filtering. The best results in every column are **bolded**. We observe that the performance of all the models is significantly degraded, especially for larger values of k .

method	top-1	top-3	top-5	top-10	top-20	top-50
MEGAN + filter	48.4	70.1	75.9	81.2	83.3	83.8
LocalRetro + filter	49.6	71.9	78.3	83.2	85.5	86.3
RetroGFN + filter	46.9	68.8	75.3	81.3	83.9	85.4
MEGAN	48.7	72.3	79.5	86.7	91.0	93.5
LocalRetro	51.5	76.5	84.3	91.0	94.9	96.7
RetroGFN	49.2	73.3	81.1	88.0	92.2	95.3

Table 10: Top-k round-trip accuracy results on USPTO-50k for models that use the Chemformer-Train filtering. The best results in every column and group are **bolded**. We observe that the performance of all the models is significantly improved, however with the price of degrading the top-k accuracy results.

method	top-1	top-3	top-5	top-10	top-20	top-50
MEGAN + filter	95.0	92.8	90.8	85.3	71.5	37.0
LocalRetro + filter	96.6	94.8	93.5	90.3	82.7	48.8
RetroGFN + filter	96.1	94.9	93.9	91.4	86.4	57.2
MEGAN	87.0	80.7	76.5	68.5	58.2	41.7
LocalRetro	93.0	87.6	84.6	79.3	71.0	54.2
RetroGFN	91.7	88.2	85.6	81.1	74.8	63.5

D Limitations and Discussion

This section briefly discusses the limitations of the paper.

D.1 Round-trip Accuracy

The main limitation of the top-k round-trip accuracy is that it relies on the forward reaction prediction model which suffers both false negative and false positive errors. However, we believe that there is an inherent epistemic uncertainty within the notion of feasibility (we cannot screen all the reactions) and any sensible retrosynthesis metric will have some portion of false negatives (it will not take all feasible reactions into account). In comparison to top-k accuracy, our round-trip accuracy has a strictly lower number of false negatives, while keeping false positives on a decent level. We believe that the round-trip will benefit from the further improvements of the forward reaction prediction model and we leave it for future work.

D.2 RetroGFN

Top-k Accuracy. The main limitation of our RetroGFN method is its results on top-k accuracy for $k < 5$. At first glance, it looks like a trade-off necessary to achieve excellent results on the round-trip accuracy. We argue that it may be caused by two things: 1) other hyperparameters of the model are not optimal for top-k accuracy, 2) the GFlowNet framework struggles with spiky reward function, and 3) the parametrization of the composition process is sub-optimal. It is possible that further refinements of the method could improve the results.

Leveraging Chemformer-Train. The fact that RetroGFN leverages the Chemformer-Train checkpoint can be seen as an unfair advantage because a similar Chemformer-Eval model is used in the round-trip accuracy computation. However, we think that fairness comes from the fact that all models use the same data splits for training or evaluation. The models differ in the way they learn from the training data and leveraging the Chemformer-Train is yet another way of learning. It does not inject any new knowledge that cannot be extracted from the training data. Once the round-trip accuracy metric is established, it becomes reasonable to optimize it using Chemformer-Train. Moreover, we believe that Chemformer-Eval and Chemformer-Train are expected to be similar because they have similar goals: 1) to extract as much information from the train and test split as possible, and 2) to extract as much information from the train split as possible. It is sensible then that they share architecture. The difference should come from the data split used for training.

E Computational Resources

We ran all the experiments on Nvidia V100 and A100 GPUs. The training of our model takes no more than 48h per checkpoint. When experimenting with the architecture and different feasibility proxy models, we trained no more than 100 checkpoints. For all the baselines, we used already trained checkpoints and only evaluated them on USPTO-50k and USPTO-MIT. The evaluation time depends on the model, but in total, it took no more than 400 GPU hours. It gives the upper bound of 5200 GPU hours for the total experimenting costs.